

Semantically Consistent Video Inpainting with Conditional Diffusion Models

Dylan Green^{1,2}, William Harvey¹, Saeid Naderiparizi^{1,2}, Matthew Niedoba^{1,2},
Yunpeng Liu^{1,2}, Xiaoxuan Liang^{1,2}, Jonathan Lavington^{1,2}, Ke Zhang^{1,2},
Vasileios Lioutas^{1,2}, Setareh Dabiri², Adam Scibior², Berend Zwartsenberg²,
and Frank Wood^{1,2}

¹ University of British Columbia, ² Inverted AI

Abstract. Current state-of-the-art methods for video inpainting typically rely on optical flow or attention-based approaches to inpaint masked regions by propagating visual information across frames. While such approaches have led to significant progress on standard benchmarks, they struggle with tasks that require the synthesis of novel content that is not present in other frames. In this paper, we reframe video inpainting as a conditional generative modeling problem and present a framework for solving such problems with conditional video diffusion models. We highlight the advantages of using a generative approach for this task, showing that our method is capable of generating diverse, high-quality inpaintings and synthesizing new content that is spatially, temporally, and semantically consistent with the provided context.

Keywords: Video Inpainting · Diffusion Models · Generative Modeling

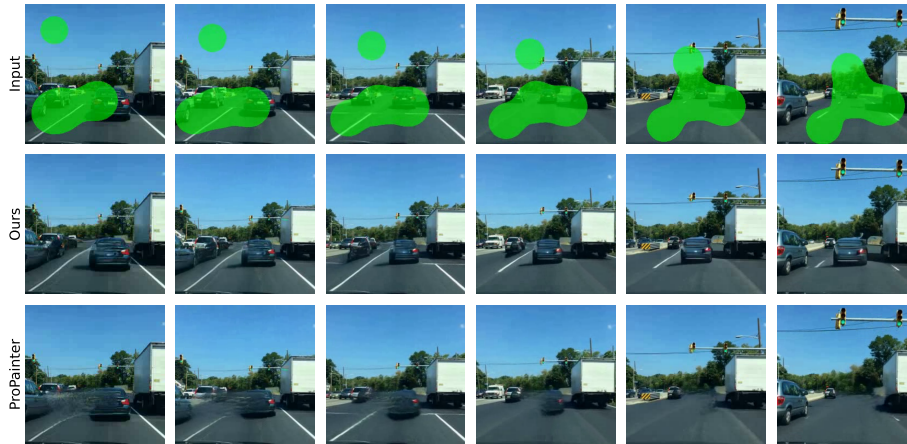


Fig. 1: Inpainting results on a task from our BDD-Inpainting dataset. The first row shows the input to the model, with the occlusion mask marked in green. Our method (second row) is capable of generating a plausible completion of the partly occluded vehicle and realistically propagating it through time. On the contrary, in the result from the best-competing method, ProPainter [52] (third row), the inpainted vehicle quickly fades away and is not modeled in a semantically consistent manner.

1 Introduction

Video inpainting is the task of filling in missing pixels in a video with plausible values. It has many practical applications in video editing and visual effects, including video restoration [32], object or watermark removal [21], and video stabilization [19]. High-quality video inpainting requires that the content of inpainted spatiotemporal regions blend seamlessly with the provided context. While significant progress has been made on image inpainting in recent years [18, 22, 26, 30, 43, 45], video inpainting remains a challenging task due to the added time dimension, which drastically increases computational complexity and leads to a stricter notion of what it means for an inpainting to be plausible. Specifically, inpainted regions require not only per-frame spatial and semantic coherence as in image inpainting, but also temporal coherence between frames and realistic motion of objects in the scene.

Despite these difficulties, a number of methods have been proposed in recent years which yield impressive results. The most successful amongst these explicitly attempt to inpaint masked regions by exploiting visual information present in other frames, typically using optical flow estimates [3, 10, 12, 15, 40] or attention-based approaches [14, 16, 20, 44] to determine how this information should be propagated across frames. Such methods implicitly assume that the information needed to fill in masked regions is present in neighboring frames, which is not the case in a variety of inpainting tasks. For example, inpainting tasks where an object is partially or fully occluded for the duration of the video (as in Fig. 1) require the method to synthesize novel content that cannot be borrowed from other frames, indicating that strong generative capabilities are required for the general task of video inpainting.



Fig. 2: An example inpainting task from our Traffic-Scenes dataset.

Further, prior work has overlooked the utility of the *semantic* content of the video being inpainted, an understanding of which is particularly important for tasks where inpainting effectively amounts to inferring the behavior of occluded objects. To illustrate this, consider Fig. 2. The black car at the top of the roundabout enters the masked region (shown in green) shortly after the first frame, and emerges some seconds later near the bottom of the frame. For an inpainting to be plausible, the car must follow a realistic trajectory around the roundabout. Note that, without a strong prior, there is insufficient information in the context to determine what such a trajectory might look like; the model must have

some notion of what makes a vehicle trajectory plausible at a semantic level. For the roundabout example above, this includes, for instance, that vehicles should remain on the road surface, that vehicles travel forward with respect to their orientation, *etc.* To accomplish this, the model must also correctly observe the entry and exit points of the vehicle, which could be arbitrarily far apart from each other in the general case. Additionally, the video inpainting problem is ill-posed – given the events observed in the context, there exists a diversity of plausible trajectories the car could take, and video inpainting methods should account for this. As such, we assert that video inpainting methods must be capable of incorporating semantic knowledge, modeling long-range dependencies, and generating diverse solutions to solve the general video inpainting problem.

We argue that a sensible approach to video inpainting is to learn a conditional distribution over possible inpaintings given the observed context. Indeed, generative approaches to image inpainting using GANs [30, 43, 45], autoregressive models [22], and diffusion models [18, 26] have long been amongst the top performing methods for image inpainting, and are capable of generating diverse, semantically coherent outputs. Such an approach has recently been made possible by the development of diffusion models for video [5, 8, 9, 35, 41], which are capable of generating long, temporally coherent, photorealistic samples. In this work, we present a framework for using conditional video diffusion models for video inpainting. We demonstrate how to use long-range temporal attention to generate semantically consistent behaviour of inpainted objects over long time horizons, even when our model cannot be jointly model all frames due to memory constraints. We can do this even for inpainted objects that have no or limited visibility in the context, a quality not present in the current literature. We report strong experimental results on several challenging video inpainting tasks, outperforming state-of-the-art approaches on a range of standard metrics.

2 Related Work

Video Inpainting Recent advances in video inpainting have largely been driven by methods which fill in masked regions by borrowing content from the unmasked regions of other frames. These methods typically use optical flow estimates [3, 10, 12, 40], self-attention [14, 16, 20, 44] or a combination of both [15, 47, 52] to determine how to propagate pixel values or learned features across frames. Such methods often produce visually compelling results, particularly on tasks where the mask-occluded region is visible in nearby frames such as foreground object removal. They struggle, however, in cases where this does not hold, *e.g.* in the presence of heavy camera motion, large masks, or tasks where semantic understanding of the video content is required to produce a convincing result.

More recent work has utilized diffusion models for video inpainting. Chang *et al.* [1] uses a latent diffusion model [24, 34] to remove the agent’s view of itself from egocentric videos for applications in robotics. Notably, this is framed as an image inpainting task, where the goal is to remove the agent (with a mask provided by a segmentation model) from a single video frame conditioned on h pre-

vious frames. Consequently, the results lack temporal consistency when viewed as videos, and the model is evaluated using image inpainting metrics only. Zhang *et al.* [51] proposes a method for the related task of text-conditional video inpainting, which produces impressive results but requires user intervention. Most similar to this work, Gu *et al.* [4] proposes a method for video inpainting that combines a video diffusion model with optical flow guidance.

Image Inpainting with Diffusion Models This work takes inspiration from the recent success of diffusion models for image inpainting. These methods can be split into two groups: those that inpaint using an unconditional diffusion model by making heuristic adjustments to the sampling procedure [18, 46], and those that explicitly train a conditional diffusion model which, if sufficiently expressive and trained to optimality, enables exact sampling from the conditional distribution [26, 48]. We follow the latter approach in this work.

3 Background

Conditional Diffusion Models A conditional diffusion model [7, 28, 33] is a generative model parameterized by a neural network trained to remove noise from data. The network is conditioned on $t \in \{1, \dots, T\}$, an integer describing how much noise has been added to the data. Given hyperparameters $1 > \bar{\alpha}_1 > \dots > \bar{\alpha}_T > 0$, training data is created by multiplying the original data by a factor $\sqrt{\bar{\alpha}_t}$ and then adding unit Gaussian noise ϵ scaled to have variance $(1 - \bar{\alpha}_t^2)$. The network should then map from this noisy data, the timestep t , and conditioning input \mathbf{y} , to a prediction of the added noise ϵ . It is trained with the squared error loss

$$\mathcal{L}(\theta) := \mathbb{E}_{t, \mathbf{x}, \mathbf{y}, \epsilon} \left[\left\| \epsilon - \epsilon_\theta \left(\sqrt{\bar{\alpha}_t} \mathbf{x} + \sqrt{1 - \bar{\alpha}_t} \epsilon, \mathbf{y}, t \right) \right\|^2 \right], \quad (1)$$

where $\epsilon_\theta(\dots)$ is the output of the network. Data \mathbf{x} and \mathbf{y} are sampled from the data distribution p_{data} , and the timestep t is typically sampled from a pre-specified categorical distribution. Once such a “denoising” network has been trained, various methods exist for using it to draw approximate samples from $p_{\text{data}}(\mathbf{x}|\mathbf{y})$ [7, 11, 28, 29, 33]. We use the Heun sampler proposed by Karras *et al.* [11], and leave further details to the appendix.

Video Diffusion Models Before we discuss conditional video diffusion models, we first discuss video diffusion models in general. A number of recent papers have proposed diffusion-based approaches to generative modeling of video data [5, 8, 9, 35, 41]. We follow the majority of these approaches [5, 8, 35] in using a 4-D U-Net [25] architecture to parameterize $\epsilon_\theta(\dots)$. Alternating spatial and temporal attention blocks within the U-Net capture dependencies within and across frames respectively, with relative positional encodings [27, 38] providing information about each frame’s position within the video. Due to computational constraints, video diffusion models are inherently limited to conditioning on and generating a small number of frames at a time, which we denote as K .

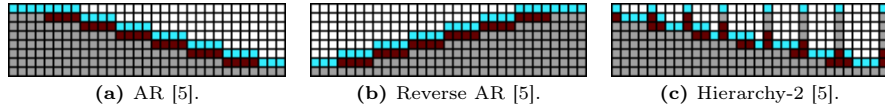


Fig. 3: Sampling schemes for generating videos of length $N = 31$ while accessing only $K = 8$ frames at a time. Each row of each subfigure depicts a different stage of our sampling process, starting from the top row and working down. Each column represents one video frame. Within each stage, frames shown in cyan are being sampled conditioned on the values of previously-sampled frames shown in dark red. Frames shown in white are not yet generated. By the end, all frames are generated and shown in light gray.

Flexible Video Diffusion Models Generating long videos with numbers of frames $N \gg K$ then requires sampling from the diffusion model multiple times. A typical approach would be to break the generation down into multiple stages, and in each stage sample $K/2$ frames conditioned on the previous $K/2$ frames. We depict this approach in Fig. 3a, with each row representing one stage. A problem with this strategy is that it fails to capture dependencies on frames more than $K/2$ frames in the past. Alternative orders in which to generate frames (which we will refer to as “sampling schemes”) are possible, with some additional ones depicted in Figs. 3b and 3c. Each of these sampling schemes tends to have its downsides, and experimentation usually requires expensive retraining of models. Harvey *et al.* [5] therefore suggest training a single model that can perform well on any sampling scheme. In particular, they train a model to generate any subset of video frames conditioned on any other subset with the objective

$$\mathcal{L}_{\text{flexible}}(\theta) := \mathbb{E}_{t, \mathbf{x}, \mathbf{y}, \mathcal{X}, \mathcal{Y}, \epsilon} \left[\left\| \epsilon - \epsilon_{\theta} \left(\sqrt{\bar{\alpha}_t} \mathbf{x} + \sqrt{1 - \bar{\alpha}_t} \epsilon, \mathbf{y}, \mathcal{X}, \mathcal{Y}, t \right) \right\|^2 \right], \quad (2)$$

in which \mathbf{x} are the frames to remove noise from at indices \mathcal{X} , and \mathbf{y} are the frames to condition on at indices \mathcal{Y} . To sample \mathbf{x} and \mathbf{y} we first sample \mathcal{X} and \mathcal{Y} , then sample a training video, and then extract the frames at indices \mathcal{X} and \mathcal{Y} to form \mathbf{x} and \mathbf{y} , respectively. Both the number of frames to generate and the number to condition on can vary, so the shapes of \mathbf{x} , ϵ , and \mathbf{y} can vary correspondingly. The network is given the indices of all frames (\mathcal{X} and \mathcal{Y}), as they are used to create the relative positional encodings [27, 38]. Once a network is trained to make predictions for arbitrary indices \mathcal{X} given arbitrary indices \mathcal{Y} , it can be used to sample long videos with any desired sampling scheme. Sampling schemes will henceforth be denoted as $\{\mathcal{X}_s, \mathcal{Y}_s\}_{s=1}^S$ where S is the number of sampling stages and, at stage s , \mathcal{X}_s and \mathcal{Y}_s are the indices of the latent and observed frames, respectively.

4 Video Inpainting with Conditional Diffusion Models

4.1 Problem Formulation

We consider the problem of creating an N -frame video \mathbf{V} conditioned on some subset of known pixel values specified by a pixel-level mask \mathbf{M} . Entries of \mathbf{M} take

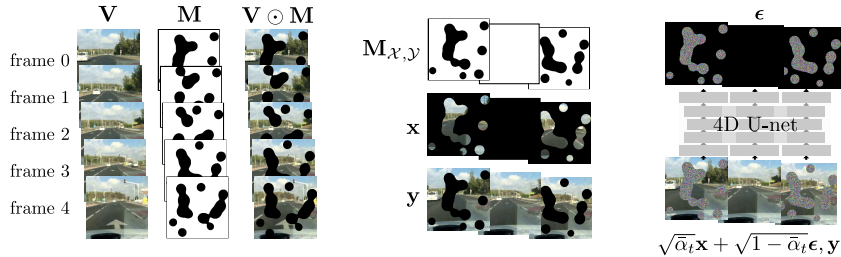


Fig. 4: Example model inputs during training. **Left:** Visualizations of a 5-frame video \mathbf{V} , a corresponding mask \mathbf{M} , and the resulting known pixel values $\mathbf{V} \odot \mathbf{M}$. **Center:** Collated training inputs if $\mathcal{X} = [0, 3]$ and $\mathcal{Y} = [2]$. The observations in \mathbf{y} are then the whole of frame 2 and known pixel values in frames 0 and 3. The task is to predict the unknown pixel values in frames 0 and 3. **Right:** Inputs fed to the neural network, with noise added to pixel values in \mathbf{x} but not those in \mathbf{y} . The task is then to predict the noise ϵ . For simplicity we do not show inputs t , $\mathbf{M}_{\mathcal{X}, \mathcal{Y}}$, or $\mathcal{X} \oplus \mathcal{Y}$.

value 1 where the corresponding pixel in \mathbf{V} is known and take 0 elsewhere. We frame this as a conditional generative modeling problem, where we aim to learn an approximation of the posterior under the data distribution $p_{\theta}(\mathbf{V}|\mathbf{V} \odot \mathbf{M}) \approx p_{\text{data}}(\mathbf{V}|\mathbf{V} \odot \mathbf{M})$, with \odot defined such that $a \odot \mathbf{M}$ returns the set of elements in a for which the corresponding value in \mathbf{M} is 1.

Recall that, due to constraints from the network architecture, Harvey *et al.* [5] were restricted to conditioning on or generating at most K frames at a time. In the video inpainting problem we are predicting and conditioning on pixels rather than frames, but our network architecture imposes an analogous constraint: we can only predict or condition on pixels from at most K different frames at a time. We modify the definition of a sampling scheme from Harvey *et al.* [5] as follows: we again denote sampling schemes $\{\mathcal{X}_s, \mathcal{Y}_s\}_{s=1}^S$ with \mathcal{X}_s and \mathcal{Y}_s being collections of frame indices. Now, however, at each stage we sample values for only unknown pixels in frames indexed by \mathcal{X}_s , and condition on known pixel values in all frames indexed by either \mathcal{X}_s or \mathcal{Y}_s . Referencing Fig. 5, in each row (stage) we show frames indexed by \mathcal{X}_s in cyan and frames indexed by \mathcal{Y}_s in either dark red or bright red. Frames shown in bright red contain missing pixels, which we do not wish to sample or condition on until a later sampling stage; we describe how we deal with this in Sec. 4.4.

4.2 Architecture

We generalize the FDM architecture of Harvey *et al.* [5] to use pixel-level masks rather than frame-level masks, as in the image inpainting approach proposed by Saharia *et al.* [26]. Concretely, every input frame is concatenated with a mask which takes value 1 where the corresponding pixel is observed and 0 elsewhere. The input values are clean (without added noise) for observed pixels and noisy values otherwise.



Fig. 5: Sampling schemes visualizations similar to Fig. 3. In addition we now also condition on observed pixel values in frames that can also contain unknown pixel values. Frames where we do so are shown in **bright red** and the color scheme is otherwise the same as in Fig. 3.

4.3 Training Procedure

Recall that we wish to train a model that can generate plausible values for unknown pixels in frames indexed by \mathcal{X} , conditioned on known pixel values in frames indexed by either \mathcal{X} or \mathcal{Y} . We simulate such tasks by first sampling a video \mathbf{V} and a mask \mathbf{M} from our dataset, and then sampling frame indices \mathcal{X} and \mathcal{Y} from a “frame index distribution” similar to that of Harvey *et al.* [5].¹ The distribution over masks \mathbf{M} can be understood as reflecting the variability in the types of masks we will encounter at test-time, and the frame index distribution can be understood as reflecting our desire to be able to sample from the model using arbitrary sampling schemes. Given \mathbf{M} , \mathcal{X} , and \mathcal{Y} , we create a combined list of frames $\mathcal{X} \oplus \mathcal{Y}$, where \oplus denotes concatenation, and a corresponding mask $\mathbf{M}_{\mathcal{X},\mathcal{Y}} := \mathbf{M}[\mathcal{X}] \oplus \mathbf{1}[\mathcal{Y}]$, where $\mathbf{1}[\mathcal{Y}]$ is a mask of all 1’s for each frame indexed in \mathcal{Y} . This masks only the missing pixels in frames \mathcal{X} while treating all pixels in frames \mathcal{Y} as observed (visualized in Fig. 4). We then extract our training targets from the video as $\mathbf{x} := \mathbf{V}[\mathcal{X} \oplus \mathcal{Y}] \odot (1 - \mathbf{M}_{\mathcal{X},\mathcal{Y}})$, and our observations as $\mathbf{y} := \mathbf{V}[\mathcal{X} \oplus \mathcal{Y}] \odot \mathbf{M}_{\mathcal{X},\mathcal{Y}}$.

Resampling \mathbf{V} , \mathbf{M} , \mathcal{X} , and \mathcal{Y} for every training example therefore defines a distribution over \mathbf{x} and \mathbf{y} , which we use when estimating the expectation over them in Eq. (2). Combining this method of sampling \mathbf{x} and \mathbf{y} with our pixel-wise mask, we write the loss as

$$\mathcal{L}_{\text{ours}}(\theta) := \mathbb{E}_{t,\mathbf{x},\mathbf{y},\mathcal{X},\mathcal{Y},\epsilon} \left[\left\| \epsilon - \epsilon_{\theta} \left(\sqrt{\bar{\alpha}_t} \mathbf{x} + \sqrt{1 - \bar{\alpha}_t} \epsilon, \mathbf{y}, \mathbf{M}_{\mathcal{X},\mathcal{Y}}, \mathcal{X} \oplus \mathcal{Y}, t \right) \right\|^2 \right], \quad (3)$$

where $\mathcal{X} \oplus \mathcal{Y}$ provides information about each frame’s index within \mathbf{V} , and $\mathbf{M}_{\mathcal{X},\mathcal{Y}}$ is the mask making explicit which pixels have known values.

4.4 Inpainting Long Videos

Given the architecture and training procedure we have described so far, we can use the resulting models to to implement the AR and Hierarchy-2 sampling schemes shown in Figs. 3a and 3c without further complication. A downside of

¹ Our frame index distribution is a mixture distribution between the one used by Harvey *et al.* [5] and one which always samples \mathcal{X} and \mathcal{Y} so that they represent sequences of consecutive frames. We found that including these sequences of consecutive frames improved temporal coherence.

these sampling schemes, however, is that they do not enable us to condition on frames with unknown pixel values. That is, we are not able to condition on the known pixels in a frame unless we either (a) have previously inpainted it and know all of its pixel values already, or (b) are inpainting it as we condition on it. We show in our experiments that this often leaves us unable to account for important dependencies in the context.

We therefore propose a method for conditioning on *incomplete* frames. This enables the sampling schemes shown in Fig. 5, where we condition on the known pixels in incomplete frames, marked in **red**. Recall that \mathbf{x} denotes “unknown pixels in frames indexed by \mathcal{X} ” and \mathbf{y} denotes “known pixels in frames indexed by \mathcal{X} or \mathcal{Y} ”. If any frames indexed by \mathcal{Y} are incomplete then we have a third category, which we’ll call \mathbf{z} : “unknown pixels in frames indexed by \mathcal{Y} ”.

We then wish to approximately sample $\mathbf{x} \sim p_{\text{data}}(\cdot|\mathbf{y})$ without requiring values of \mathbf{z} . We do not have a way to sample directly from an approximation of this distribution, as the diffusion model is not trained to condition on “incomplete” frames. We note, however, that this desired distribution is the marginal of a distribution that our diffusion model *can* approximate:

$$p_{\text{data}}(\mathbf{x}|\mathbf{y}) = \int p_{\text{data}}(\mathbf{x}, \mathbf{z}|\mathbf{y})d\mathbf{z} \approx \int p_{\theta}(\mathbf{x}, \mathbf{z}|\mathbf{y})d\mathbf{z}. \quad (4)$$

This means that we can sample from the required approximation of $p_{\text{data}}(\mathbf{x}|\mathbf{y})$ by sampling from $p_{\theta}(\mathbf{x}, \mathbf{z}|\mathbf{y})$ and then simply discarding \mathbf{z} .

4.5 Sampling Schemes

The ability to condition on incomplete frames enables us to design new sampling schemes that better capture dependencies that are necessary for high-quality video inpainting. **Improved AR** is a variant of AR that takes into account information from future frames by conditioning on the observed parts of the frames immediately after the sequence of frames being generated, as well as on the frames before; see Fig. 5a. **Improved AR w/ Far Future** builds on “Improved AR” by conditioning on the observed parts of frames far in the future instead of of frames immediately after those being sampled; see Fig. 5b. **3-Resolution Improved AR** (3-Res. Improved AR) builds on “Improved AR” by first infilling every fifteenth frame using Improved AR, then infilling every fifth frame while conditioning on nearby infilled frames, and then infilling all other frames. We visualize a “2-res.” version (infilling every third frame and then every frame) in Fig. 5c. Visualizations of all sampling schemes considered in this work can be found in Appendix C.

5 Experiments

5.1 Datasets

To highlight the unique capabilities our generative approach offers, we wish to target video inpainting tasks in which visual information in nearby frames cannot be easily exploited to achieve a convincing result. The YouTube-VOS [39]

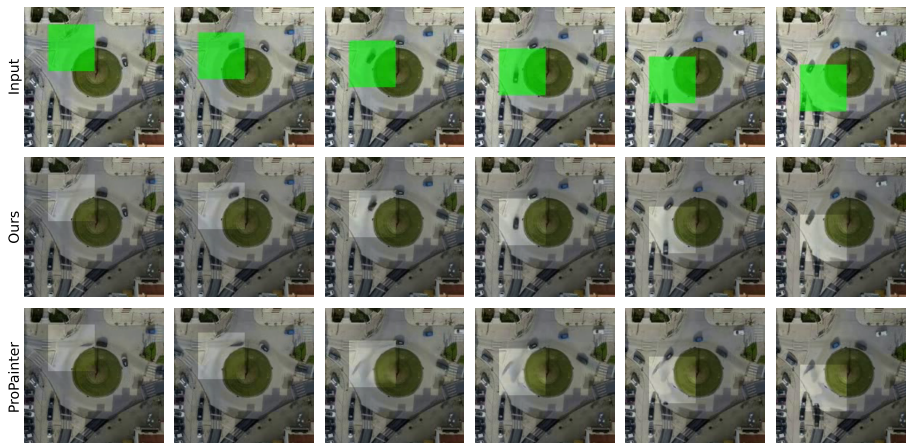


Fig. 6: Inpaintings from our model and ProPainter on the task introduced in Fig. 2 from our Traffic-Scenes dataset. Our model can inpaint a realistic trajectory for the occluded vehicle. Competing flow-based approaches correctly inpaint the background but are unable to account for the vehicle.

(training and test) and DAVIS [23] (test) video object segmentation datasets have become the *de facto* standard benchmark datasets for video inpainting in recent years, and the foreground object masks included in these datasets have led to a heavy focus on object removal tasks in qualitative evaluations of video inpainting methods. Object removal in these datasets is a task to which *e.g.* optical flow-based approaches are specifically well suited, as the backgrounds are often near-stationary and so information in neighboring frames can be used to great effect. In contrast, we wish to focus on tasks where inpainting requires the visual appearances of objects to be hallucinated in whole or in part and realistically propagated through time, or where the behavior of occluded objects must be inferred. We propose four new large-scale video inpainting datasets targeting such tasks. All datasets are 256×256 resolution and 10 fps. Representative examples of each dataset, along with details of how each dataset was constructed, are included in Appendix D.

BDD-Inpainting We adapt the BDD100K [42] dataset for the video inpainting task. This dataset contains 100,000 high-quality first-person driving videos and includes a diversity of geographic locations and weather conditions. We select a random subset of approximately 50,000 of these, and generate a set of both moving and stationary masks of four types: grids, horizontal or vertical lines, boxes (Fig. 6), and blobs (Fig. 1). During training both videos and masks are sampled uniformly, giving a distribution over an extremely varied set of inpainting tasks. We include two test sets of 100 video-mask pairs each, the first (BDD-Inpainting) containing only grid, line, and box masks, and the second (BDD-Inpainting-Blobs) containing only blob masks. The second is a substan-



Fig. 7: Inpainted videos from our Inpainting-Background dataset. Results from our method are displayed on the top row; results from the best competing model FGT [47] are on the bottom row. The ground truth region is darkened slightly to aid in visualizing the boundary between generated and ground-truth regions. Despite FGT outperforming our method on quantitative metrics, qualitative results are similar in quality.

tially more challenging test set, as the masks are often large and occlude objects in the scene for a significant period of time. See the appendix for representative examples. The test sets we use, along with code for processing the original BDD100K dataset and generating masks, will be released upon publication.

Inpainting-Cars and Inpainting-Background We use an in-house dataset of overhead drone footage of vehicle traffic, for which we have tracker-generated bounding boxes for each vehicle, to create two task-specific datasets. The first, Inpainting-Background (Fig. 7), targets the removal of cars from videos by using time-shifted bounding boxes as occlusion masks, where the bounding boxes are shifted such that the masked-out region contains only the road surface and other environmental factors. The second, Inpainting-Cars (Fig. 8), targets the *addition* of cars to videos by using the original bounding boxes as masks so that the masked-out region always contains a single vehicle. Note that the masked-out vehicle is not visible at any time in the context, and so, given an input, the model must hallucinate a vehicle and propagate it through time, using only the size and movement of the mask as clues to plausible vehicle appearance and motion.

Traffic Scenes Using the same in-house dataset as referenced above, we generate another dataset where large sections of the roadway are occluded, requiring the model to infer vehicle behavior in the masked-out region. Crops are centered over road features like intersections, roundabouts, highway on-ramps, *etc.* where complex vehicle behavior and interactions take place. This dataset contains exceptionally challenging video inpainting tasks as vehicles are often occluded for long durations of time, requiring the model to generate plausible trajectories that are semantically consistent with both the observations (e.g. the entry and exit point of a vehicle from the masked region) and the roadway. This dataset

contains approximately 13,000 videos in the training set and 100 video-mask pairs in the test set.

5.2 Baselines and Metrics

We compare our method with four recently proposed video inpainting methods that achieve state-of-the-art performance on standard benchmarks: ProPainter [52], E²FGVI [15], FGT [47], and FGVC [3]. For each model, we use pre-trained checkpoints made available by the respective authors. We adopt the evaluation suite of DEVIL [31], which includes a comprehensive selection of commonly used metrics targeting three different aspects of inpainting quality:

- Reconstruction, or how well the method’s output matches the ground truth: PSNR, SSIM [37], LPIPS [49], PVCS [31].
- Perceptual realism, or how well the appearance and/or motion resembles a reference set of ground truth videos: FID [6], VFID [36].
- Temporal consistency: Flow warping error (E_{warp}) [13], which measures how well an inpainting follows the optical flow as calculated on the ground truth.

For our method, we train one model on each dataset with $K = 16$. Models are trained on $4 \times$ NVIDIA A100 GPUs for 1-4 weeks. A detailed accounting of each model’s hyperparameters and training procedure can be found in the appendix.

5.3 Quantitative Evaluation

We report quantitative results across four of our datasets in Table 1. For each dataset, we report metrics for the best-performing model and sampling scheme we found for that dataset. For all metrics other than E_{warp} our method outperforms the baselines on three out of four datasets, often by a significant margin. We suspect the discrepancy between E_{warp} and the other metrics is because each of the competing methods predicts a completion of the optical flow field and utilizes this during the inpainting process, in a sense explicitly targeting E_{warp} . On the Infilling-Background dataset the baseline methods dominate, likely owing to this being precisely the kind of task that flow-based propagation is well-suited to; the (approximate) ground truth is visible in neighbouring frames. Infilling-Cars is omitted from this section, as we are not aware of an existing method suitable for this task.

5.4 Qualitative Evaluation

BDD-Inpainting On this dataset, qualitative differences between our method and competing approaches are most evident in the presence of large masks that partially or fully occlude objects for a long period of time or the entire video. In such cases our method can retain or complete the visual appearance of occluded objects and propagate them through time in a realistic way, while such objects tend to disappear gradually with flow-based approaches (as in Fig. 1).

Table 1: Quantitative comparison with state-of-the-art video inpainting methods across each of our four datasets. For each dataset/metric, the best performing model is indicated with bold font and the second best performing model is underlined. Improved AR w/ Far Future is used for all datasets but Inpainting-Background, which uses AR.

| Method | PSNR \blacktriangle | SSIM \blacktriangle | LPIPS \blacktriangledown | PVCS \blacktriangledown | FID \blacktriangledown | VFID \blacktriangledown | E_{warp} \blacktriangledown |
|-----------------------|-----------------------|-----------------------|----------------------------|---------------------------|--------------------------|---------------------------|--------------------------------------|
| BDD-Inpainting | | | | | | | |
| ProPainter | <u>32.65</u> | <u>0.968</u> | <u>0.0355</u> | <u>0.2806</u> | <u>2.51</u> | <u>0.1599</u> | 1.5$\cdot 10^{-3}$ |
| FGT | 28.50 | 0.928 | 0.0843 | 0.6430 | 9.94 | 0.7863 | 4.0 $\cdot 10^{-3}$ |
| E ² FGVI | 30.16 | 0.946 | 0.0640 | 0.4765 | 6.58 | 0.3665 | 2.3 $\cdot 10^{-3}$ |
| FGVC | 25.84 | 0.884 | 0.1498 | 1.0210 | 32.08 | 1.7995 | 7.5 $\cdot 10^{-3}$ |
| Ours | 33.68 | 0.972 | 0.0261 | 0.2037 | 1.71 | 0.0748 | <u>1.8$\cdot 10^{-3}$</u> |
| BDD-Inpainting-Blobs | | | | | | | |
| ProPainter | <u>30.54</u> | <u>0.960</u> | <u>0.0467</u> | <u>0.3120</u> | <u>2.56</u> | <u>0.1499</u> | 1.2$\cdot 10^{-3}$ |
| FGT | 27.33 | 0.938 | 0.0737 | 0.5130 | 9.41 | 0.3594 | 2.5 $\cdot 10^{-3}$ |
| E ² FGVI | 29.04 | 0.950 | 0.0667 | 0.4414 | 4.23 | 0.2339 | 1.7 $\cdot 10^{-3}$ |
| FGVC | 25.10 | 0.913 | 0.0980 | 0.6957 | 16.64 | 0.6184 | 3.8 $\cdot 10^{-3}$ |
| Ours | 30.67 | 0.961 | 0.0442 | 0.2857 | 1.69 | 0.1083 | <u>1.5$\cdot 10^{-3}$</u> |
| Inpainting-Background | | | | | | | |
| ProPainter | 42.03 | <u>0.994</u> | 0.0145 | 0.0572 | 2.83 | <u>0.0550</u> | 2.6$\cdot 10^{-4}$ |
| FGT | 44.23 | 0.996 | 0.0081 | 0.0371 | 1.35 | 0.0462 | <u>2.9$\cdot 10^{-4}$</u> |
| E ² FGVI | 37.27 | 0.985 | 0.0400 | 0.2074 | 6.71 | 0.2600 | 6.0 $\cdot 10^{-4}$ |
| FGVC | <u>42.92</u> | 0.993 | <u>0.0117</u> | <u>0.0557</u> | <u>1.99</u> | 0.0742 | 4.7 $\cdot 10^{-4}$ |
| Ours | 38.99 | 0.987 | 0.0273 | 0.1443 | 6.11 | 0.1455 | 4.1 $\cdot 10^{-4}$ |
| Traffic-Scenes | | | | | | | |
| ProPainter | <u>31.98</u> | <u>0.967</u> | <u>0.0326</u> | <u>0.2909</u> | <u>8.51</u> | <u>0.3482</u> | <u>2.5$\cdot 10^{-4}$</u> |
| FGT | 31.97 | 0.963 | 0.0397 | 0.3528 | 9.92 | 0.5392 | 3.6 $\cdot 10^{-4}$ |
| E ² FGVI | 31.40 | 0.957 | 0.0440 | 0.3809 | 13.13 | 0.6113 | 4.1 $\cdot 10^{-4}$ |
| FGVC | 29.11 | 0.926 | 0.0794 | 0.5914 | 25.93 | 1.2358 | 9.9 $\cdot 10^{-4}$ |
| Ours | 35.29 | 0.978 | 0.0202 | 0.1725 | 4.87 | 0.1637 | 2.3$\cdot 10^{-4}$ |

Qualitative results on this dataset are heavily influenced by the sampling scheme used. Our ‘‘Improved AR w/ Far Future’’ sampling scheme tends to perform best, as it allows us to incorporate information from both past and future frames in the inpainting process. See Appendix F.2 for a qualitative demonstration of the effects of different sampling schemes.

Traffic-Scenes On this dataset, all competing methods tend to inpaint only the road surface; when vehicles enter the occluded region they disappear almost instantaneously. Our method shows a surprising ability to inpaint long, realistic trajectories that are consistent with the entry/exit points of vehicles into the occluded region, as well as correctly following roadways as in Fig. 6.

Inpainting-Background Qualitatively, all methods perform similarly on this dataset. Specifically, regardless of which method is used, it is difficult to tell where the masked region is without a visual aid on most inpainted videos (see Fig. 7). In some examples where the ground stays stationary for an extended period of time, our method produces artifacts that are likely to contribute to its poor performance on this dataset compared to the others.

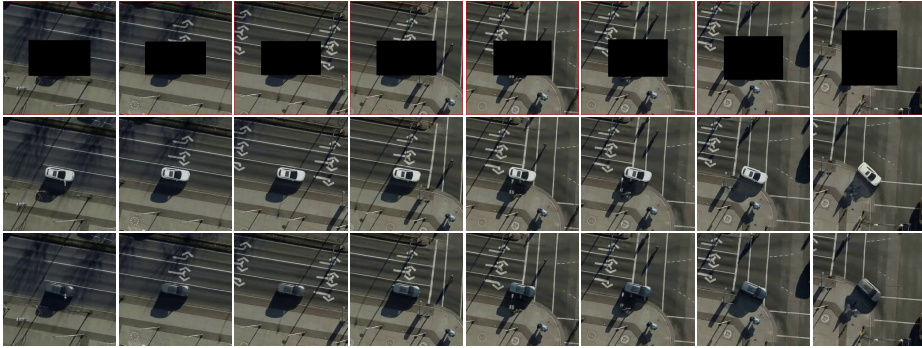


Fig. 8: Inpaintings from our model on the Inpainting-Cars dataset. The first row is the masked input to the model, the lower two rows are two separate inpaintings sampled from our model.

Inpainting-Cars Sampled inpaintings from our model on an example from the Inpainting-Cars dataset are shown in Fig. 8. Our model is capable of generating diverse, visually realistic inpaintings for a given input. We note the model’s ability to use *semantic* cues from the context to generate plausible visual features, such as realistic behavior of shadows and plausible turning trajectories based only on the movement of the mask.

5.5 Ablations

Effect of Sampling Schemes We compare selected sampling schemes on the Traffic-Scenes dataset in Table 2, before providing more thorough qualitative and quantitative comparisons in the appendix. Improved AR w/ Far Future is the best on all datasets aside from Infilling-Background in terms of video realism (VFID) and temporal consistency (warp error), demonstrating the importance of our method’s ability to condition on incomplete frames. AR tends to do poorly on all metrics on both the Traffic-Scenes and BDD-Inpainting datasets. This is likely due to its inability to account for observed pixel values in frames coming after the ones being generated at each stage, causing divergence from the ground-truth and then artifacts when producing later frames conditioned on incompatible values. Hierarchy-2 does well on some metrics of reconstruction and frame-wise perceptual quality. It does less well in terms of video realism, as the inpainting of the “keyframes” in the first stage is done without conditioning on the known pixels of frames in their immediate vicinity, potentially leading to incompatibility with the local context.

Samplers and Number of Sampling Steps The use of diffusion models allows for a trade-off of computation time *vs.* inpainting quality through the number of steps used in the generative process. In Table 3 we report the results

Table 2: Effect of sampling schemes, measured on the Traffic-Scenes test set.

| Sampling Scheme | PSNR \blacktriangle | SSIM \blacktriangle | LPIPS \blacktriangledown | PVCS \blacktriangledown | FID \blacktriangledown | VFID \blacktriangledown | E_{warp} \blacktriangledown |
|---------------------------|-----------------------|-----------------------|----------------------------|---------------------------|--------------------------|---------------------------|--|
| AR | 31.72 | 0.9595 | 0.0392 | 0.2989 | 8.85 | 0.3016 | $3.01 \cdot 10^{-4}$ |
| Hierarchy-2 | 35.53 | 0.9794 | 0.0196 | 0.1732 | 4.55 | 0.1714 | $2.48 \cdot 10^{-4}$ |
| Improved AR w/ Far Future | 35.29 | 0.9783 | 0.0202 | 0.1725 | 4.87 | 0.1637 | $2.26 \cdot 10^{-4}$ |
| 3-Res. Improved AR | 35.32 | 0.9785 | 0.0210 | 0.1815 | 5.07 | 0.1821 | $2.43 \cdot 10^{-4}$ |

Table 3: Effect of diffusion samplers, using AR sampling on BDD-Inpainting.

| Sampler | PSNR \blacktriangle | SSIM \blacktriangle | LPIPS \blacktriangledown | PVCS \blacktriangledown | FID \blacktriangledown | VFID \blacktriangledown | E_{warp} \blacktriangledown |
|-------------------|-----------------------|-----------------------|----------------------------|---------------------------|--------------------------|---------------------------|--|
| Heun (10 steps) | 33.00 | 0.9687 | 0.0339 | 0.2437 | 2.39 | 0.1155 | $1.66 \cdot 10^{-3}$ |
| Heun (25 steps) | 33.05 | 0.9703 | 0.0290 | 0.2202 | 1.84 | 0.0815 | $1.78 \cdot 10^{-3}$ |
| Heun (50 steps) | 33.00 | 0.9699 | 0.0282 | 0.2177 | 1.81 | 0.0766 | $1.82 \cdot 10^{-3}$ |
| Heun (100 steps) | 32.98 | 0.9700 | 0.0280 | 0.2171 | 1.76 | 0.0788 | $1.85 \cdot 10^{-3}$ |
| DDPM (1000 steps) | 32.41 | 0.9665 | 0.0272 | 0.2244 | 1.68 | 0.0779 | $2.39 \cdot 10^{-3}$ |

of our model on the BDD-Inpainting test set with the AR sampling scheme using different samplers and numbers of sampling steps. Aligning with expectations and qualitative observations, performance on metrics degrades as the number of sampling steps decreases for LPIPS, PVCS, FID and VFID. We note, however, that performance on E_{warp} , PSNR, and SSIM improves, suggesting that these metrics may not correlate well with perceived quality, as has been previously suggested for the latter two metrics in Zhang *et al.* [50].

6 Conclusion

In this work, we have presented a framework for video inpainting by conditioning video diffusion models. This framework allows for flexible conditioning on the context, enabling post-hoc experimentation with sampling schemes which can greatly improve results. We introduce four challenging tasks for video inpainting methods and demonstrate our model’s ability to use semantic information in the context to solve these tasks effectively. Our experiments demonstrate a clear improvement on quantitative metrics and, contrary to existing methods, our approach can generate semantically meaningful completions based on minimal information in the context.

Acknowledgements We acknowledge the support of the Natural Sciences and Engineering Research Council of Canada (NSERC), the Canada CIFAR AI Chairs Program, Inverted AI, MITACS, the Department of Energy through Lawrence Berkeley National Laboratory, and Google. This research was enabled in part by technical support and computational resources provided by the Digital Research Alliance of Canada Compute Canada (alliancecan.ca), the Advanced Research Computing at the University of British Columbia (arc.ubc.ca), and Amazon.

References

1. Chang, M., Prakash, A., Gupta, S.: Look ma, no hands! agent-environment factorization of egocentric videos. In: NeurIPS (2023)
2. Chen, T.: On the importance of noise scheduling for diffusion models. arXiv preprint arXiv:2301.10972 (2023)
3. Gao, C., Saraf, A., Huang, J.B., Kopf, J.: Flow-edge guided video completion. In: Proc. European Conference on Computer Vision (ECCV) (2020)
4. Gu, B., Yu, Y., Fan, H., Zhang, L.: Flow-guided diffusion for video inpainting. arXiv preprint arXiv:2311.15368 (2023)
5. Harvey, W., Naderiparizi, S., Masrani, V., Weilbach, C.D., Wood, F.: Flexible diffusion modeling of long videos. In: NeurIPS (2022)
6. Heusel, M., Ramsauer, H., Unterthiner, T., Nessler, B., Hochreiter, S.: Gans trained by a two time-scale update rule converge to a local nash equilibrium. In: NeurIPS. pp. 6626–6637 (2017)
7. Ho, J., Jain, A., Abbeel, P.: Denoising diffusion probabilistic models. In: Advances in Neural Information Processing Systems. vol. 33, pp. 6840–6851 (2020)
8. Ho, J., Salimans, T., Gritsenko, A., Chan, W., Norouzi, M., Fleet, D.J.: Video diffusion models. arXiv:2204.03458 (2022)
9. Höppe, T., Mehrjou, A., Bauer, S., Nielsen, D., Dittadi, A.: Diffusion models for video prediction and infilling. Transactions on Machine Learning Research (2022)
10. Huang, J.B., Kang, S.B., Ahuja, N., Kopf, J.: Temporally coherent completion of dynamic video. ACM Transactions on Graphics **35**(6), 196 (2016)
11. Karras, T., Aittala, M., Aila, T., Laine, S.: Elucidating the design space of diffusion-based generative models. Advances in Neural Information Processing Systems **35**, 26565–26577 (2022)
12. Kim, D., Woo, S., Lee, J.Y., Kweon, I.S.: Deep video inpainting. In: Proceedings of the IEEE Conference on Computer Vision and Pattern Recognition. pp. 5792–5801 (2019)
13. Lai, W., Huang, J., Wang, O., Shechtman, E., Yumer, E., Yang, M.: Learning blind video temporal consistency. In: ECCV. pp. 179–195 (2018)
14. Lee, S., Oh, S.W., Won, D., Kim, S.J.: Copy-and-paste networks for deep video inpainting. In: IEEE/CVF International Conference on Computer Vision. pp. 4412–4420 (2019)
15. Li, Z., Lu, C.Z., Qin, J., Guo, C.L., Cheng, M.M.: In: IEEE Conference on Computer Vision and Pattern Recognition (CVPR) (2022)
16. Liu, R., Deng, H., Huang, Y., Shi, X., Lu, L., Sun, W., Wang, X., Dai, J., Li, H.: Fuseformer: Fusing fine-grained information in transformers for video inpainting. In: International Conference on Computer Vision (ICCV) (2021)
17. Loshchilov, I., Hutter, F.: Decoupled weight decay regularization. In: ICLR (2019)
18. Lugmayr, A., Danelljan, M., Romero, A., Yu, F., Timofte, R., Gool, L.V.: Repaint: Inpainting using denoising diffusion probabilistic models. In: IEEE/CVF Conference on Computer Vision and Pattern Recognition. pp. 11451–11461 (2022)
19. Matsushita, Y., Ofek, E., Ge, W., Tang, X., Shum, H.: Full-frame video stabilization with motion inpainting. IEEE Trans. Pattern Anal. Mach. Intell. **28**(7), 1150–1163 (2006)
20. Oh, S.W., Lee, S., Lee, J., Kim, S.J.: Onion-peel networks for deep video completion. In: IEEE/CVF International Conference on Computer Vision (2019)
21. Patwardhan, K.A., Sapiro, G., Bertalmío, M.: Video inpainting of occluding and occluded objects. In: Proceedings of the 2005 International Conference on Image Processing. pp. 69–72. IEEE (2005)

22. Peng, J., Liu, D., Xu, S., Li, H.: Generating diverse structure for image inpainting with hierarchical VQ-VAE. In: IEEE Conference on Computer Vision and Pattern Recognition. pp. 10775–10784 (2021)
23. Perazzi, F., Pont-Tuset, J., McWilliams, B., Gool, L.V., Gross, M.H., Sorkine-Hornung, A.: A benchmark dataset and evaluation methodology for video object segmentation. In: IEEE Conference on Computer Vision and Pattern Recognition. pp. 724–732 (2016)
24. Rombach, R., Blattmann, A., Lorenz, D., Esser, P., Ommer, B.: High-resolution image synthesis with latent diffusion models. In: Proceedings of the IEEE Conference on Computer Vision and Pattern Recognition (CVPR) (2022)
25. Ronneberger, O., Fischer, P., Brox, T.: U-net: Convolutional networks for biomedical image segmentation. In: International Conference on Medical image computing and computer-assisted intervention. pp. 234–241. Springer (2015)
26. Saharia, C., Chan, W., Chang, H., Lee, C.A., Ho, J., Salimans, T., Fleet, D.J., Norouzi, M.: Palette: Image-to-image diffusion models. In: SIGGRAPH. pp. 15:1–15:10 (2022)
27. Shaw, P., Uszkoreit, J., Vaswani, A.: Self-attention with relative position representations. arXiv preprint arXiv:1803.02155 (2018)
28. Sohl-Dickstein, J., Weiss, E., Maheswaranathan, N., Ganguli, S.: Deep unsupervised learning using nonequilibrium thermodynamics. In: International Conference on Machine Learning. pp. 2256–2265. PMLR (2015)
29. Song, Y., Sohl-Dickstein, J., Kingma, D.P., Kumar, A., Ermon, S., Poole, B.: Score-based generative modeling through stochastic differential equations. arXiv preprint arXiv:2011.13456 (2020)
30. Suvorov, R., Logacheva, E., Mashikhin, A., Remizova, A., Ashukha, A., Silvestrov, A., Kong, N., Goka, H., Park, K., Lempitsky, V.: Resolution-robust large mask inpainting with fourier convolutions. arXiv preprint arXiv:2109.07161 (2021)
31. Szeto, R., Corso, J.J.: The devil is in the details: A diagnostic evaluation benchmark for video inpainting. arXiv preprint arXiv:2105.05332 (2021)
32. Tang, N.C., Hsu, C., Su, C., Shih, T.K., Liao, H.M.: Video inpainting on digitized vintage films via maintaining spatiotemporal continuity. IEEE Trans. Multimed. **13**(4), 602–614 (2011)
33. Tashiro, Y., Song, J., Song, Y., Ermon, S.: CSDI: Conditional score-based diffusion models for probabilistic time series imputation. Advances in Neural Information Processing Systems **34**, 24804–24816 (2021)
34. Vahdat, A., Kreis, K., Kautz, J.: Score-based generative modeling in latent space. In: Neural Information Processing Systems (NeurIPS) (2021)
35. Voleti, V., Jolicœur-Martineau, A., Pal, C.: McVD: Masked conditional video diffusion for prediction, generation, and interpolation. In: (NeurIPS) Advances in Neural Information Processing Systems (2022)
36. Wang, T., Liu, M., Zhu, J., Yakovenko, N., Tao, A., Kautz, J., Catanzaro, B.: Video-to-video synthesis. In: NeurIPS. pp. 1152–1164 (2018)
37. Wang, Z., Bovik, A.C., Sheikh, H.R., Simoncelli, E.P.: Image quality assessment: from error visibility to structural similarity. IEEE Trans. Image Process. **13**(4), 600–612 (2004)
38. Wu, K., Peng, H., Chen, M., Fu, J., Chao, H.: Rethinking and improving relative position encoding for vision transformer. In: Proceedings of the IEEE/CVF International Conference on Computer Vision. pp. 10033–10041 (2021)
39. Xu, N., Yang, L., Fan, Y., Yue, D., Liang, Y., Yang, J., Huang, T.S.: Youtubevos: A large-scale video object segmentation benchmark. CoRR **abs/1809.03327** (2018)

40. Xu, R., Li, X., Zhou, B., Loy, C.C.: Deep flow-guided video inpainting. In: The IEEE Conference on Computer Vision and Pattern Recognition (CVPR) (June 2019)
41. Yang, R., Srivastava, P., Mandt, S.: Diffusion probabilistic modeling for video generation. arXiv:2203.09481 (2022)
42. Yu, F., Chen, H., Wang, X., Xian, W., Chen, Y., Liu, F., Madhavan, V., Darrell, T.: Bdd100k: A diverse driving dataset for heterogeneous multitask learning. In: The IEEE Conference on Computer Vision and Pattern Recognition (CVPR) (June 2020)
43. Yu, J., Lin, Z., Yang, J., Shen, X., Lu, X., Huang, T.S.: Generative image inpainting with contextual attention. In: IEEE Conference on Computer Vision and Pattern Recognition. pp. 5505–5514 (2018)
44. Zeng, Y., Fu, J., Chao, H.: Learning joint spatial-temporal transformations for video inpainting. In: The Proceedings of the European Conference on Computer Vision (ECCV) (2020)
45. Zeng, Y., Fu, J., Chao, H., Guo, B.: Aggregated contextual transformations for high-resolution image inpainting. arXiv preprint arXiv:2104.01431 (2021)
46. Zhang, G., Ji, J., Zhang, Y., Yu, M., Jaakkola, T.S., Chang, S.: Towards coherent image inpainting using denoising diffusion implicit models. In: ICML. pp. 41164–41193 (2023)
47. Zhang, K., Fu, J., Liu, D.: Flow-guided transformer for video inpainting. In: European Conference on Computer Vision. pp. 74–90. Springer (2022)
48. Zhang, L., Rao, A., Agrawala, M.: Adding conditional control to text-to-image diffusion models. In: Proceedings of the IEEE/CVF International Conference on Computer Vision. pp. 3836–3847 (2023)
49. Zhang, R., Isola, P., Efros, A.A., Shechtman, E., Wang, O.: The unreasonable effectiveness of deep features as a perceptual metric. In: CVPR (2018)
50. Zhang, R., Isola, P., Efros, A.A., Shechtman, E., Wang, O.: The unreasonable effectiveness of deep features as a perceptual metric. In: The IEEE Conference on Computer Vision and Pattern Recognition (CVPR) (2018)
51. Zhang, Z., Wu, B., Wang, X., Luo, Y., Zhang, L., Zhao, Y., Vajda, P., Metaxas, D., Yu, L.: Avid: Any-length video inpainting with diffusion model. arXiv preprint arXiv:2312.03816 (2023)
52. Zhou, S., Li, C., Chan, K.C., Loy, C.C.: ProPainter: Improving propagation and transformer for video inpainting. In: Proceedings of IEEE International Conference on Computer Vision (ICCV) (2023)

Supplementary Materials

A Limitations

The most notable limitation of our method is its computational cost relative to competing methods. The wall-clock time for our method is highly dependent on a number of factors, such as the number of sampler steps used and the number of frames generated in each stage of the sampling scheme used. Improvements in few-step generation for diffusion models and increasing the size of our model such that more frames can be processed at a time would both help to mitigate these concerns. Additionally, our method requires that a model be trained on a specific

dataset which is reasonably close to the data distribution to be inpainted at test time, requiring large datasets. The development of large scale, general purpose video generative models would likely help to make generative approaches such as ours more robust to out-of-distribution tasks.

B Potential Negative Impacts

The development of generative models for the generation of photo-realistic video opens the door to malicious or otherwise unethical uses which could have negative impacts on society. While our method is currently limited to operating on data which is sufficiently similar to the datasets it was trained on, and those datasets have limited potential for malicious use, future work which takes a generative approach to video inpainting could be used for the purposes of misinformation, harassment or deception.

C Sampling Scheme Details

Figure 9 depicts the sampling schemes used in all experiments for a video length of 200 to supplement the descriptions given in the main text.

D Dataset Details

In Appendix D.1 we detail how our datasets were generated. Appendix D.2 shows representative examples from each of our datasets.

D.1 Dataset Creation

BDD-Inpainting From the original BDD100K dataset we take a random subset of videos, using 48,886 for a training set and 100 for each held-out test set. Videos are downsampled spatially by a factor of 2.5, center-cropped to 256×256 , and the frame rate is reduced by a factor of three to 10 fps. We truncate videos to 400 frames, corresponding to a 40 second length for each. We randomly generate a set of 49,970 masks of four types: grids, horizontal or vertical lines, boxes, and blobs. Our mask generation procedure first picks a mask type, and then randomly selects mask parameters such as size and direction of motion (which includes stationary masks). Generated masks contain 400 frames. During training both videos and masks are sampled uniformly and independently, giving a distribution over nearly 2.5 billion video-mask pairs. Our test sets, as well as code for regenerating our training set, will be made public upon publication.

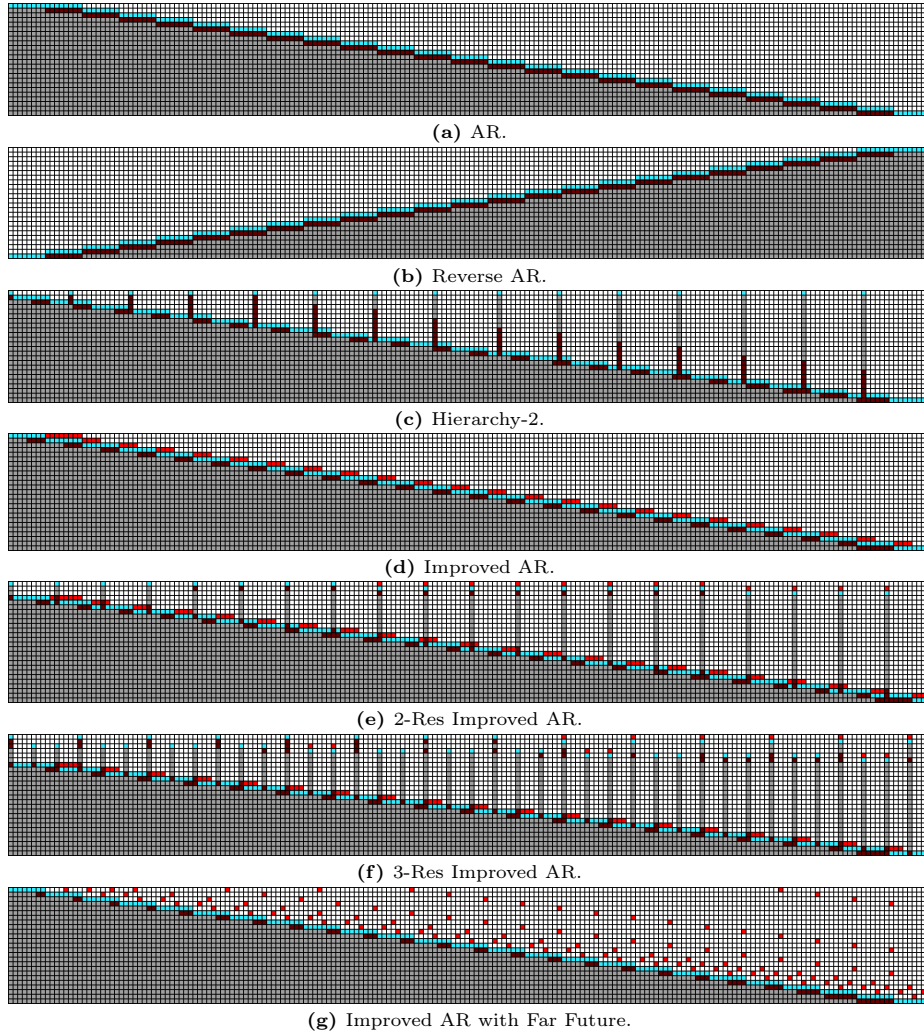


Fig. 9: Sampling schemes visualizations similar to Fig. 3 but with a model capable of attending to 16 frames at a time, as in our experiments, and a more typical video length of 200.

Inpainting-Cars We use an in-house dataset of overhead drone footage of vehicle traffic, for which we have tracker-generated bounding boxes for each vehicle. The videos are spatially downsampled by a factor of two from their original 4k resolution, and 256×256 sub-videos centred on vehicles are extracted using the vehicle-specific tracks. The length of these videos is variable as it depends on the amount of time a given vehicle was visible in the source video, but typically ranges from 10 to 60 seconds at 10 fps. Bounding boxes are dilated by a factor of two to ensure the entirety of the vehicle is contained within them,

and these dilated bounding boxes are then used as masks. This dataset contains 2973 training examples and 100 held-out test examples.

Inpainting-Background The process for creating the Inpainting-Background is nearly identical to that of Inpainting-Cars. The primary difference is that the tracks are shifted in time to find new tracks which do not intersect with the bounding box of any other vehicle, giving a dataset where the masked out region contains the road surface and other environmental factors. Beyond that, videos are processed in the same way and are of the same length as those in Inpainting-Cars. This dataset contains 2965 training examples and 100 held-out test examples.

Traffic Scenes This dataset is created using the same in-house dataset as was used for Inpainting-Cars and Inpainting-Background. The 4k, 10 fps source videos are spatially downsampled by a factor of 7.25, truncated to 200 frames and cropped to 256×256 , with the crops centred over road features like intersections, roundabouts, highway on-ramps, *etc.* We generate masks using the same mask generation procedure as in BDD-Inpainting.

D.2 Dataset Examples

BDD-Inpainting See Fig. 10 for examples from the BDD-Inpainting dataset. Mask types, shown in green, are indicated for each example.

Inpainting-Cars See Fig. 11 for examples from the Inpainting-Cars dataset. Masks are shown in black.

Inpainting-Background See Fig. 12 for examples from the Inpainting-Background dataset. Masks are shown in black.

Traffic-Scenes See Fig. 13 for examples from the BDD-Inpainting dataset. Mask types, shown in green, are indicated for each example.

E Training Details

All models are trained with $4 \times$ NVIDIA A100 GPUS with a batch size of one, corresponding to an effective batch size of 4 as gradients are aggregated across GPUs. All models were trained to condition on or generate 16 frames at a time, use an EMA rate of 0.999, and use the AdamW [17] optimizer. We use the noise schedules defined in Chen [2]: **linear** for the Inpainting-Background model, **cosine** for Inpainting-Cars, and **sigmoid** for BDD-Inpainting and Traffic-Scenes. All models use temporal attention at the spatial resolutions (32, 16, 8) in the U-Net, except for the Inpainting-Cars model where temporal attention



Fig. 10: Representative examples from the BDD-Inpainting dataset.

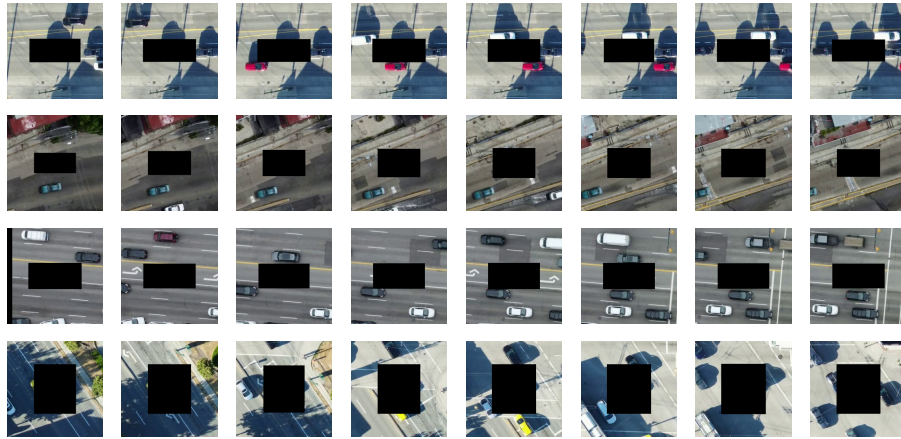


Fig. 11: Representative examples from the Inpainting-Cars dataset.

only occurs at resolutions (16, 8). Otherwise, the default hyperparameters from our training code are used for all models. This code, and the BDD-Inpainting checkpoint, will be released upon publication. The number of training iterations for each model is listed below:

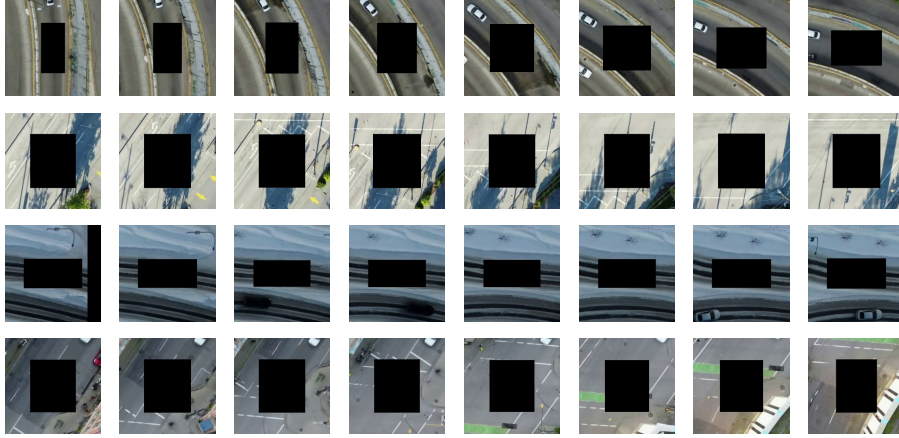


Fig. 12: Representative examples from the Inpainting-Background dataset.

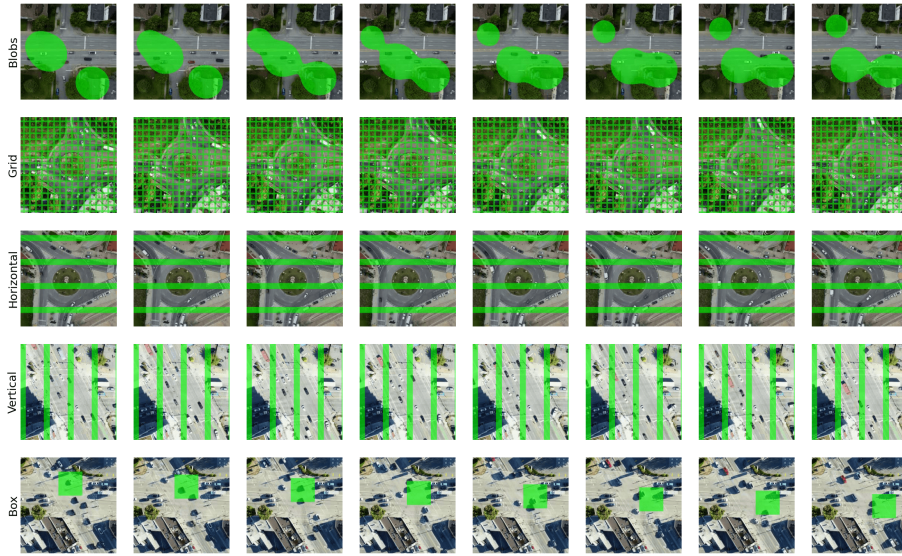


Fig. 13: Representative examples from the Traffic-Scenes dataset.

F Additional Ablations

F.1 Additional Sampling Scheme Ablations

Table 4 and Table 5 show the effect of using different sampling schemes on the BDD-Inpainting and BDD-Inpainting-Blobs test sets, respectively. The sampling

| Dataset | Iterations (millions) |
|-----------------------|-----------------------|
| BDD-Inpainting | 2.5 |
| Inpainting-Cars | 1.1 |
| Inpainting-Background | 1.5 |
| Traffic-Scenes | 2.4 |

schemes tested are depicted in Fig. 3 and Fig. 5. For each metric, the best performing sampling scheme is indicated in bold font. All measurements were taken using the Heun sampler [11] with 100 sampling steps. The Improved AR w/ Far Future performs best on both test sets across almost all metrics. Sampling scheme ablations are omitted for Inpainting-Background and Inpainting-Cars as we found an autoregressive scheme gave significantly better qualitative results than the other schemes.

Table 4: Effect of sampling schemes measured on the BDD-Inpainting test set.

| Sampling Scheme | PSNR \blacktriangle | SSIM \blacktriangle | LPIPS \blacktriangledown | PVCS \blacktriangledown | FID \blacktriangledown | VFID \blacktriangledown | $E_{\text{warp}}\blacktriangledown$ |
|---------------------------|-----------------------|-----------------------|----------------------------|---------------------------|--------------------------|---------------------------|--|
| 3-Res. Improved AR | 32.81 | 0.9678 | 0.0289 | 0.2302 | 1.75 | 0.0884 | $2.19 \cdot 10^{-3}$ |
| Improved AR w/ Far Future | 33.68 | 0.9717 | 0.0261 | 0.2037 | 1.71 | 0.0748 | $1.79 \cdot 10^{-3}$ |
| AR | 32.97 | 0.9699 | 0.0278 | 0.2166 | 1.78 | 0.0778 | $1.85 \cdot 10^{-3}$ |
| Hierarchy-2 | 32.96 | 0.9690 | 0.0284 | 0.2232 | 1.74 | 0.0839 | $1.97 \cdot 10^{-3}$ |
| 2-Res. Improved AR | 33.18 | 0.9692 | 0.0278 | 0.2201 | 1.72 | 0.0815 | $2.03 \cdot 10^{-3}$ |
| Reverse AR | 33.31 | 0.9702 | 0.0273 | 0.2132 | 1.76 | 0.0785 | $1.79 \cdot 10^{-3}$ |

Table 5: Effect of sampling schemes measured on the BDD-Inpainting-Blobs test set.

| Sampling Scheme | PSNR \blacktriangle | SSIM \blacktriangle | LPIPS \blacktriangledown | PVCS \blacktriangledown | FID \blacktriangledown | VFID \blacktriangledown | $E_{\text{warp}}\blacktriangledown$ |
|---------------------------|-----------------------|-----------------------|----------------------------|---------------------------|--------------------------|---------------------------|--|
| 3-Res. Improved AR | 29.89 | 0.9561 | 0.0475 | 0.3142 | 1.63 | 0.1188 | $2.00 \cdot 10^{-3}$ |
| Improved AR w/ Far Future | 30.67 | 0.9608 | 0.0442 | 0.2857 | 1.69 | 0.1083 | $1.53 \cdot 10^{-3}$ |
| AR | 29.45 | 0.9547 | 0.0512 | 0.3319 | 2.07 | 0.1328 | $1.61 \cdot 10^{-3}$ |
| Hierarchy-2 | 29.97 | 0.9570 | 0.0474 | 0.3106 | 1.65 | 0.1137 | $1.74 \cdot 10^{-3}$ |
| 2-Res. Improved AR | 30.25 | 0.9583 | 0.0454 | 0.2991 | 1.59 | 0.1116 | $1.79 \cdot 10^{-3}$ |
| Reverse AR | 30.04 | 0.9590 | 0.0450 | 0.2920 | 1.8 | 0.1134 | $1.51 \cdot 10^{-3}$ |

F.2 Qualitative Sampling Scheme Ablations

In this section we highlight the qualitative impact that different sampling schemes can have on the quality of inpainted videos. We select a video from the test set where conditioning on the appropriate frames is crucial for our method to succeed. Figure 14 shows the beginning of this video, where a car is occluded in the right-hand lane for the first few seconds of the video (see input frames in the first row). The Autoregressive scheme (second row) shows a distinct “pop-in”

effect, as when the initial frames were generated the model was not able to condition on future frames where the cars existence and appearance are revealed. Both Reverse-Autoregressive and AR w/ Far Future (third and fourth rows) do condition on future frames that contain the car; Reverse-Autoregressive because the model is able to propagate the car backwards through time, and AR w/ Far Future because the model conditions on frames far out into the future where the car has been revealed. Figure 15 shows the end of the video, where the cars in the right-hand lane are occluded and remain occluded for the rest of the video (first row). The Autoregressive scheme keeps these cars visible, as it is able to propagate them forward through time (second row). Reverse-Autoreg (third row) fails for the same reason that Autoreg did at the beginning: when the final frames were generated, the model was not able to condition on frames where the vehicles were visible. AR w/ Far Future (fourth row) is again successful; despite the cars not becoming visible again (and thus there is no “future” to condition on), it is able to propagate the cars forward in time as the Autoreg scheme does. We provide an mp4 video showing the entire inpainting for this video using the sampling schemes discussed here and more in the supplementary, with filename `appendix_E2.mp4`. Sampling schemes used in each tile are labelled in the video.

G Diffusion Model Sampling Details

As alluded to in the main paper, we train a diffusion model that uses ϵ -prediction to parameterize the score of a distribution over \mathbf{x}_t at each time t . This can be used to parameterize a stochastic differential equation (or ordinary differential equation) that morphs samples from a unit Gaussian into approximate samples from the conditional distribution of interest $p_{\text{data}}(\mathbf{x}|\mathbf{y})$ [29]. We use the Heun sampler proposed by [11] to integrate this SDE. Our hyperparameters are $\sigma_{\text{max}} = 1000$, $\sigma_{\text{min}} = 0.002$, $\rho = 7$, $S_{\text{churn}} = 80$, $S_{\text{max}} = \infty$, $S_0 = 0$, and $S_{\text{noise}} = 1$. We use 100 sampling steps (involving 199 network function evaluations) for each experiment except where specified otherwise.

H Additional Qualitative Results

BDD-Inpainting Figure 16 and Figure 17 show additional results on tasks from the BDD-Inpainting test set.

Traffic-Scenes Figure 18 and Figure 19 show additional results on tasks from the Traffic-Scenes training set.

Inpainting-Cars Figure 20 shows additional results on tasks from the Traffic-Scenes training set.

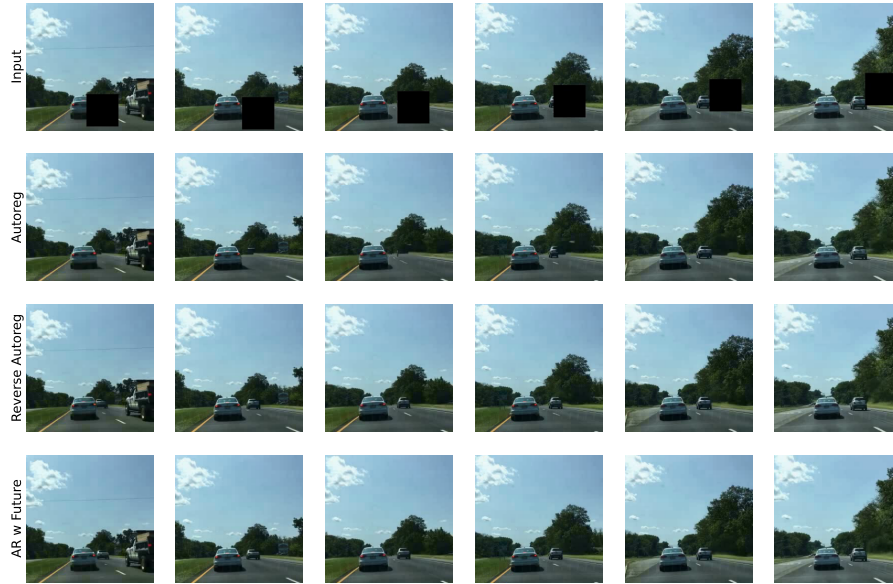


Fig. 14: Qualitative results from different sampling schemes on the beginning of the video discussed in Appendix F.2

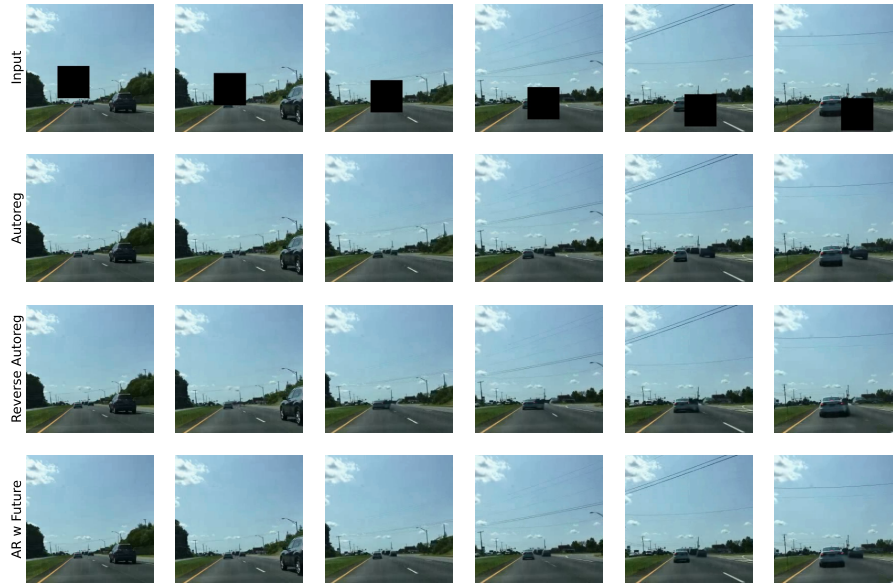


Fig. 15: Qualitative results from different sampling schemes on the end of the video discussed in Appendix F.2



Fig. 16: Qualitative results from our method and all the competing methods we compared to quantitatively on an example from the BDD-Inpainting test set. We note that, in the presence of small masks, the qualitative differences are less pronounced between our method and the best-performing benchmarks, like since information in neighbouring frames can more easily be exploited. For our method we use the Improved AR w/ Far Future sampling scheme.

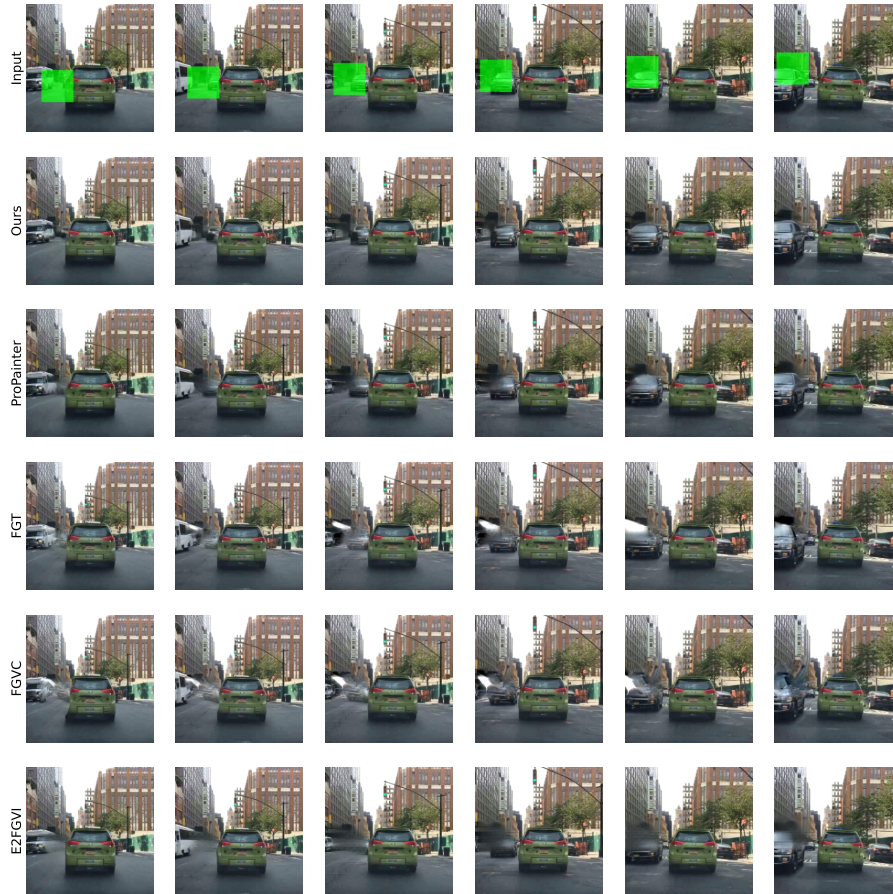


Fig. 17: Qualitative results from our method and all the competing methods we compared to quantitatively on an example from the BDD-Inpainting test set. Again, for our method we use the Improved AR w/ Far Future sampling scheme. In this video the vehicle passing in the left-hand lane is only ever partially visible, causing other methods to produce blurry results.

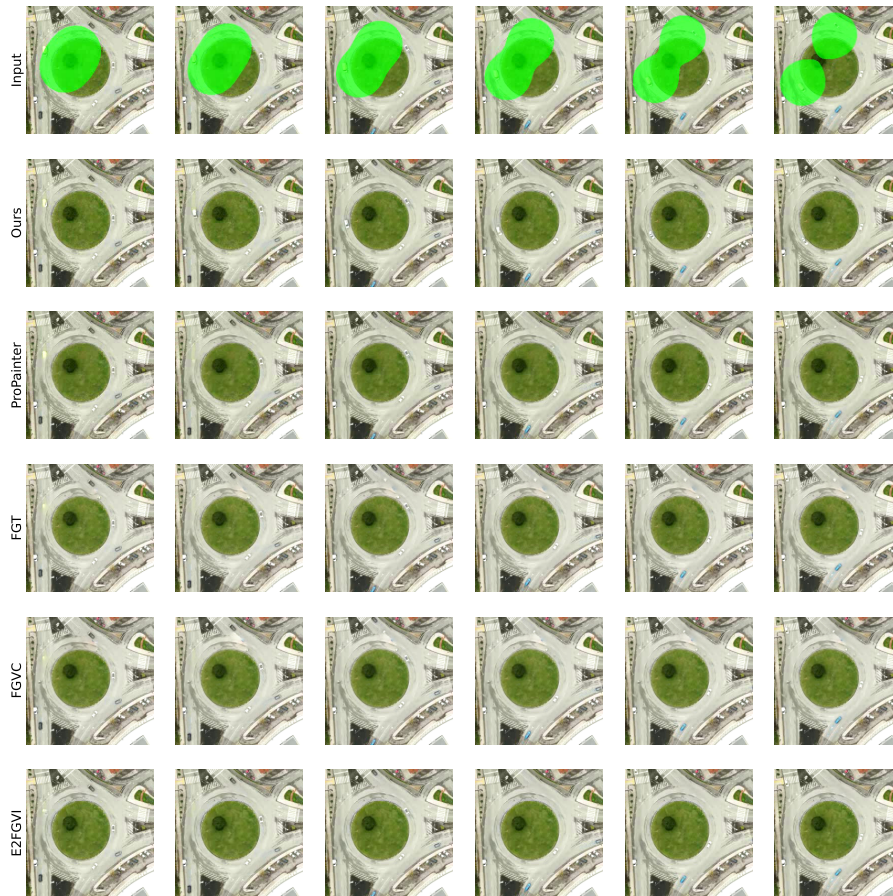


Fig. 18: Qualitative results from our method and all the competing methods we compared to quantitatively on an example from the Traffic-Scenes test set. For our method we use the Hierarchy-2 sampling scheme. For our method the two occluded vehicles are inpainted with continuous trajectories; for all other methods the vehicles disappear while they are occluded.



Fig. 19: Further qualitative results from our method and all the competing methods we compared to quantitatively on an example from the Traffic-Scenes test set. In the ground truth for this example, in the first frame there is a vehicle making a left hand turn towards the bottom of the image that is occluded until it briefly emerges many frames later. Our model is able to initialize a vehicle in the inpainting and complete a trajectory which is consistent with the exit point for the vehicle. In all other methods the vehicle appears suddenly.

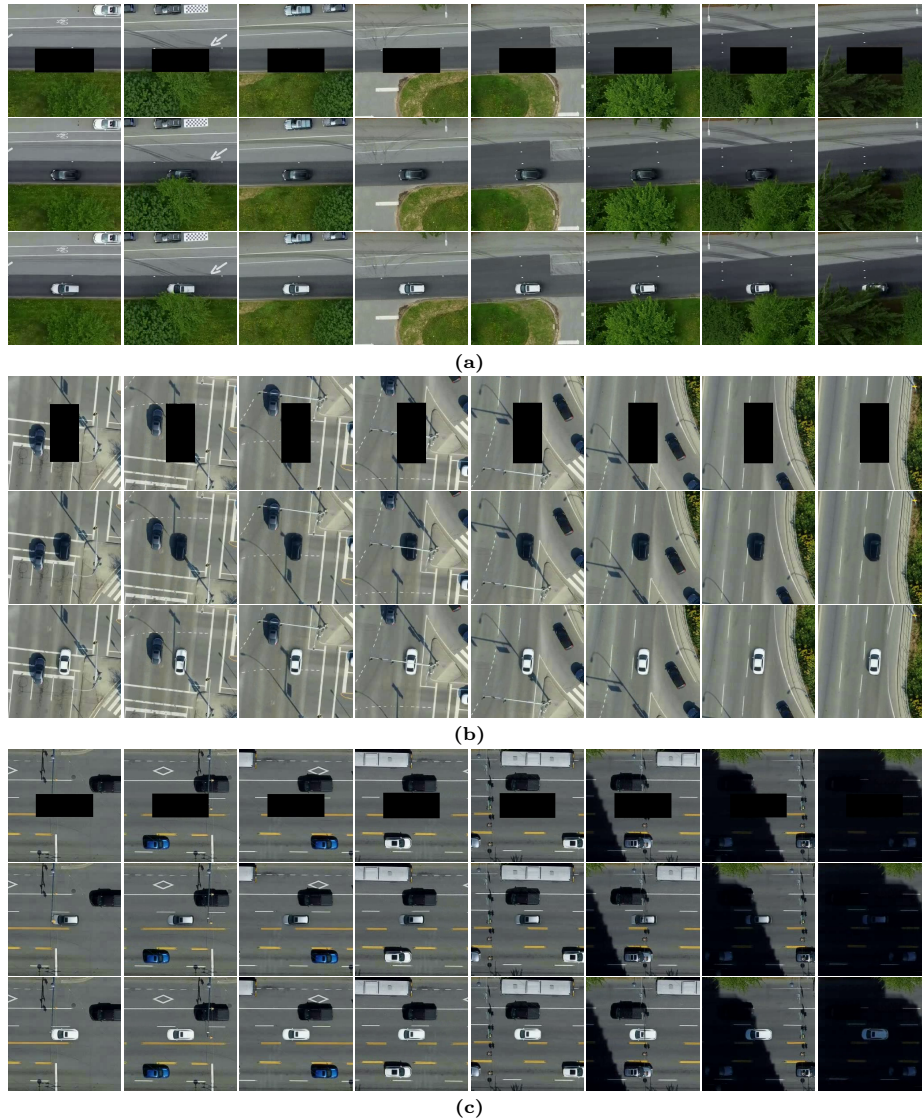


Fig. 20: Additional qualitative results from our method on the Inpainting-Cars test set, demonstrating our method’s ability to generate diverse vehicle appearances to inpaint the scene and to deal with various complications in the context. In Fig. 20a, our method is able to deal with partial occlusion by trees in the scene. In Fig. 20b, note that the inpainted cars’ shadows are oriented in the same direction as the shadows of other objects. Fig. 20c demonstrates that our method is capable of realistically shading an inpainted vehicle’s color when it enters the shade.